Proceeding of the IEEE
International Conference on Robotics and Biomimetics
Dali, China, December 2019

Dimension Reduced Instantaneous Inverse Kinematics for Configuration Variable Limits of Continuum Manipulators*

Zhonghao Wu, *Student Member*, *IEEE*
UM-SJTU Joint Institute

Haozhe Yang, Xu Liu, and Kai Xu†, *Member*, *IEEE*
School of Mechanical Engineering

Shanghai Jiao Tong University
Shanghai, China

{zhonghao.wu, silence1004, xu.liu, & k.xu}@sjtu.edu.cn

Abstract **- Continuum manipulators gain popularity and have been applied in various scenarios due to their advantages such as design compactness, dexterity, intrinsic compliance, etc. Since analytical inverse kinematics for a continuum manipulator with constant-length segments does not exist, numerical approaches, such as resolved motion rates, are usually adopted. A good practice shall ensure numerical stability for the configuration variables near their limits. However, the existing methods mainly focus on preventing the configuration variables from saturation. When an updated configuration variable violates its limit in an inverse kinematics process, the updated variable is simply bounded at the corresponding limit. This handling approach sometimes leads to a position and (or) orientation divergence. This paper hence proposes a dimension reduced instantaneous inverse kinematics for the configuration variable limits of non-redundant continuum manipulators. This dimension reduction method is enabled by the configuration variables that are not at their limits to achieve numerical stability during the entire inverse kinematics process. Numerical Experimental simulations are reported on a 6-DoF (Degree of Freedom) continuum manipulator. A clear improvement was identified while compared with the conventional Jacobian-based numerical inverse kinematics.**

Index Terms **– Continuum Manipulator, Configuration Variable, Inverse Kinematics, Joint Limit, Jacobian Matrix,.**

I. Introduction

Continuum manipulators have segments that can bend continuously and appear smooth curves [1]. Due to the distinct characteristics like structural simplicity, intrinsic compliance, dexterity and design compactness [2-4], continuum manipulators are showing great potentials in industrial inspection, minimally invasive surgery, prosthetics, etc.

Current approaches for formulating the kinematics of continuum segments mainly include the following five methods, via i) the uses of Hamilton's principle, ii) elliptic integrals, iii) Cosserat rod theory, iv) virtual power, and v) constant curvature bending assumption. The constant curvature bending assumption treats a bent segment as a circular arc and this handling is computationally efficient and has been well verified theoretically and experimentally [2, 5].

Under this constant curvature bending assumption, each circular arc can be defined via three configuration variables: bending angle, bending plane direction, and continuum segment length. With the target poses expressed in the task space, the inverse kinematics from the task space to the configuration space of the continuum manipulator does not have analytical solutions with constant-length segments [6]. The inverse kinematics usually adopts a Jacobian-based resolved motion rates solution [7]. Implementation examples include the 6-DoF (Degree of Freedom) manipulator in a previous study [8], as shown in Fig. 1, and several others [9-11].

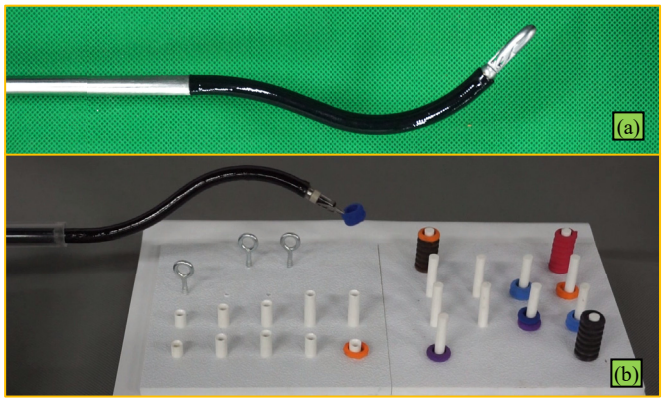

Fig. 1 (a) A constructed 6-DoF continuum manipulator from [8]; (b) the continuum manipulator performing a peg transfer task.

It is expected that this iterative inverse kinematics process always maintains its numerical stability for the configuration variables of the continuum manipulator even around their limits. Handling the configuration variable limits (joint limits) usually include the following approaches. For example, a weighted least-norm solution can be used to penalize the motion towards joint limits [12]. On the other hand, extended Jacobian matrix can be used to push the joint values towards their range centers [13]. However, these methods cannot guarantee the avoidance of reaching the joint limits. When an updated joint value violates the corresponding limit, the joint value is usually bounded at its limit. Sometimes, this simplistic handling leads to position and (or) orientation

*This work was supported in part by the National Key R&D Program of China (Grant No. 2017YFC0110800), and in part by the National Natural Science Foundation of China (Grant No. 51722507, Grant No. 51435010 and Grant No. 91648103).

978-1-7281-6321-5/19//$31.00 ©2019 IEEE

divergence. Such a divergence phenomenon is illustrated in Section IV in detail.

Recent developments proposed null space saturation algorithm [14] and joint clamping algorithm [15] for kinematically redundant manipulators. Inspired by these developments, this paper hence presents a dimension reduced instantaneous inverse kinematics for continuum manipulators, aiming at achieving numerically stable real-time teleoperation. The fundamental principle lies on the use of the unsaturated configuration variables to realize the desired position and orientation tasks.

What's more, the end effector orientation of a continuum manipulator is highly coupled with the end effector position due to its bent body shapes. When the position and the orientation inverse kinematics cannot converge at the same time, a prioritized formulation is adopted with tip position assigned with a higher priority.

The remainder of this paper is organized as follows. Section II explains the dimension reduced instantaneous inverse kinematics, while the kinematics modeling of a 6-DoF continuum manipulator is derived in Section III. Experimental characterizations are reported in Section IV with the conclusions summarized in Section V.

II. Dimension Reduction with Scaling

The algorithm background is briefly introduced in Section II.A, while the proposed dimension reduction is elaborated in Section II.B in detail.

A. Resolved Motion Rate Control

An n-DoF continuum manipulator is assumed for an m-dimension task space pose $\mathbf{x}$ (generally $n \geq 6$, $m = 6$), the Jacobian for the manipulator can be expressed as follows.

$$\mathbf{J} = \begin{bmatrix} \mathbf{j}_1 & \cdots & \mathbf{j}_i & \cdots & \mathbf{j}_n \end{bmatrix} \tag{1}$$

Where $\mathbf{j}_i$ is the column vector representing the partial derivative of the end effector twist $\mathbf{x}$ with respect to the i-th configuration variable ψ_i of the configuration vector $\boldsymbol{\psi}$.

Jacobian matrix can establish instantaneous kinematics mapping from the configuration velocity $\dot{\boldsymbol{\psi}}$ to the task velocity $\dot{\mathbf{x}}$. The instantaneous kinematics is formulated as follows.

$$\dot{\mathbf{x}} = \mathbf{J}\dot{\boldsymbol{\psi}} \tag{2}$$

$$\dot{\boldsymbol{\psi}} = \mathbf{J}^{\dagger}\dot{\mathbf{x}} = \mathbf{J}^{\dagger}\begin{bmatrix} \mathbf{v}^T & \boldsymbol{\omega}^T \end{bmatrix}^T \tag{3}$$

Where $\dot{\mathbf{x}}$ is a six-dimension twist vector, with the first three elements defining the linear velocity $\mathbf{v}$ and the last three for the angular velocity $\boldsymbol{\omega}$; $\mathbf{J}^{\dagger}$ is the Moore–Penrose pseudoinverse inverse matrix of $\mathbf{J}$.

The flowchart of the resolved motion rate control, from [7], is illustrated in Fig. 2. $\mathbf{v}$ and $\boldsymbol{\omega}$ are determined by the current position error $\varepsilon_{\mathbf{p}}$ and orientation error $\varepsilon_{\mathbf{R}}$. The expressions are as follows.

$$\begin{cases} \varepsilon_{\mathbf{p}} = \left\| \mathbf{p}_t - \mathbf{p}_c \right\| \\ \varepsilon_{\mathbf{R}} = \mathrm{rot}_{\theta}^{-1}\left(\mathbf{R}_t \mathbf{R}_c^T \right) \end{cases} \tag{4}$$

$$\begin{cases} \mathbf{v} = v_{\mathbf{x}\lim}\left(\mathbf{p}_t - \mathbf{p}_c \right) / \left\| \mathbf{p}_t - \mathbf{p}_c \right\| \\ \boldsymbol{\omega} = \omega_{\mathbf{x}\lim}\, \mathrm{rot}_{\hat{\mathbf{r}}}^{-1}\left(\mathbf{R}_t \mathbf{R}_c^T \right) \end{cases} \tag{5}$$

Where $\mathbf{p}_t$ and $\mathbf{R}_t$ are the target position and orientation, respectively. $\mathbf{p}_c$ and $\mathbf{R}_c$ are the current position and orientation. The operators of $\mathrm{rot}_{\theta}^{-1}(\mathbf{R})$ and $\mathrm{rot}_{\hat{\mathbf{r}}}^{-1}(\mathbf{R})$ give the angle and the axis of a rotation matrix $\mathbf{R}$. $v_{\mathbf{x}\lim}$ and $\omega_{\mathbf{x}\lim}$ are preset constant scalars for maximal linear and angular velocities.

Since $\dot{\boldsymbol{\psi}}$ can be obtained from (3), the configuration vector $\boldsymbol{\psi}$ is updated as in (6) for each iteration, where Δt is the time interval.

$$\boldsymbol{\psi} = \boldsymbol{\psi} + \Delta t \dot{\boldsymbol{\psi}} \tag{6}$$

The pose is then updated through forward kinematics. The iteration will continue until the $\varepsilon_{\mathbf{p}}$ and $\varepsilon_{\mathbf{R}}$ are less than the error thresholds (or the number of the iterations exceeds a preset value).

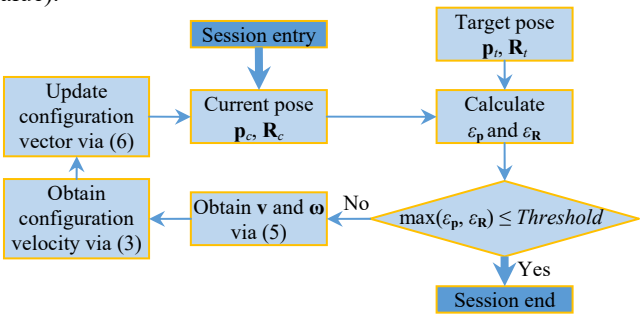

Fig. 2 Flowchart of the resolved motion rate control.

B. Dimension Reduction

When a configuration variable violates its limit, it is usually bounded at the limit. However, this can be problematic and it is elaborated as follows. Eq. (2) can be rewritten as in Eq. (7), using Eq. (1).

$$\dot{\mathbf{x}} = \begin{bmatrix} \mathbf{v}^T & \boldsymbol{\omega}^T \end{bmatrix}^T = \sum_{i=1}^{n} \mathbf{j}_i \dot{\psi}_i \tag{7}$$

During an inverse kinematics process, the configuration variable ψ_a is assumed to violate the corresponding limit $\psi_{a\lim}$ in the next iteration (with a step of $\dot{\psi}_a \Delta t$). If this configuration variable is simply bounded at the limit, the task velocity (a.k.a., end effector twist) is actually as follows:

$$\dot{\mathbf{x}}_{\mathrm{act}} = \begin{bmatrix} \mathbf{v}_{\mathrm{act}}{}^T & \boldsymbol{\omega}_{\mathrm{act}}{}^T \end{bmatrix}^T = \begin{bmatrix} \mathbf{v}^T & \boldsymbol{\omega}^T \end{bmatrix}^T - \mathbf{j}_a \left(\dot{\psi}_a - \frac{\psi_{a\lim} - \psi_a}{\Delta t} \right) \tag{8}$$

Generally, $\dot{\mathbf{x}}_{\mathrm{act}}$ and $\dot{\mathbf{x}}$ are not along the same direction. When the deviation is large enough, the inverse kinematics may start to diverge, resulting in increasing position or orientation errors.

The method's fundamental is to discard the a^{th} configuration variable that reaches its own limit, and only use the rest joints to realize a partial inverse kinematics mapping from the task space to the configuration space. With the a^{th} configuration variable fixed at the last iteration value, the continuum manipulator has its number of DoFs reduced.

The reduced Jacobian matrix $\tilde{\mathbf{J}}$ is then obtained by removing the corresponding column vector $\mathbf{j}_a$:

$$\tilde{\mathbf{J}} = \begin{bmatrix} \mathbf{j}_1 & \cdots & \mathbf{j}_{a-1} & \mathbf{j}_{a+1} & \cdots & \mathbf{j}_n \end{bmatrix} \tag{9}$$

The dimension of each column vector $\mathbf{j}_i$ keeps unchanged. The instantaneous inverse kinematics is then to find a modified inverse kinematics mapping from the task space velocity to the reduced configuration space.

When the number of the remaining configuration variables is less than the dimension of the desired task vector $[\mathbf{v}^T\ \boldsymbol{\omega}^T]^T$, the linear velocity and angular velocity may not be satisfied simultaneously. Linear velocity is set at a higher priority with respect to the angular velocity. Then a prioritized-Jacobian formulation is adopted to generate the configuration velocity with reduced dimension $\dot{\tilde{\boldsymbol{\psi}}}$ [16].

$$\dot{\tilde{\boldsymbol{\psi}}} = \tilde{\mathbf{J}}_{\mathbf{v}}^{\dagger}\mathbf{v} + [\tilde{\mathbf{J}}_{\boldsymbol{\omega}}(\mathbf{I} - \tilde{\mathbf{J}}_{\mathbf{v}}^{\dagger}\tilde{\mathbf{J}}_{\mathbf{v}})]^{\dagger}(\boldsymbol{\omega} - \tilde{\mathbf{J}}_{\boldsymbol{\omega}}\tilde{\mathbf{J}}_{\mathbf{v}}^{\dagger}\mathbf{v}) \tag{10}$$

Where $\tilde{\mathbf{J}}_{\mathbf{v}}$ and $\tilde{\mathbf{J}}_{\boldsymbol{\omega}}$ are from $\tilde{\mathbf{J}} = \begin{bmatrix} \tilde{\mathbf{J}}_{\mathbf{v}}^T & \tilde{\mathbf{J}}_{\boldsymbol{\omega}}^T \end{bmatrix}^T$, representing the modified linear and angular velocity mapping, respectively.

During each iteration, if there are more than one configuration variables reach their limits, the reduced configuration velocity can also be similarly derived via discarding these configuration variables at the same time.

As the iterative inverse kinematics process continues, an updated configuration velocity may still lead to the remaining configuration variables violating their limits. Then the dimension of the dimension-reduced Jacobian needs to be further reduced, until all the calculated configuration variables are within their limits.

In order to improve numerical stability caused by possible singularity, a singularity robust formulation was adopted for the pseudoinverse matrix as in Eq. (11).

$$\mathbf{J}^{\dagger} = \mathbf{J}^T\left(\mathbf{J}\mathbf{J}^T + \lambda\mathbf{I}\right)^{-1} \tag{11}$$

Where λ is a constant damping coefficient.

Besides the singularity robust formulation, a scaling-down procedure is integrated to avoid excessive configuration velocities. The scaling-down coefficient is to make sure the obtained configuration velocities are within the manipulator's motion capability. The coefficient is obtained as in Eq. (12).

$$s = \min\left(\left|\frac{v_{p1}}{\dot{\psi}_{p1}}\right|, \left|\frac{v_{p2}}{\dot{\psi}_{p2}}\right|, \ldots, \left|\frac{\omega_{r1}}{\dot{\psi}_{r1}}\right|, \left|\frac{\omega_{r2}}{\dot{\psi}_{r2}}\right|, \ldots, 1\right) \tag{12}$$

Where $\dot{\psi}_{p1}$, $\dot{\psi}_{p2}$, … are the prismatic configuration velocities, and $\dot{\psi}_{r1}$, $\dot{\psi}_{r2}$, … are the revolute configuration velocities. v_{p1}, v_{p2}, …, ω_{r1}, ω_{r2}, … are the corresponding maximal configuration velocities.

Thereafter, the dimension-reduced configuration vector $\tilde{\boldsymbol{\psi}}$ is updated as in (13).

$$\tilde{\boldsymbol{\psi}} = \tilde{\boldsymbol{\psi}} + s\Delta t\dot{\tilde{\boldsymbol{\psi}}} \tag{13}$$

A flowchart for the implementation of the dimension reduction inverse kinematics in a single iteration is shown in Fig. 3, ensuring the configuration variables are all within their limits and constrain the modified configuration velocities within their feasible ranges.

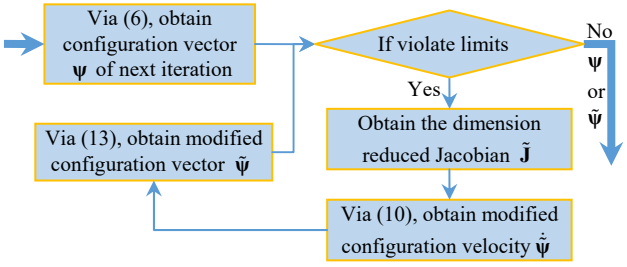

Fig. 3 Flowchart of the dimension-reduced method.

III. Kinematics

The dimension reduced inverse kinematics was applied to a 2-segment continuum manipulator. The continuum segments are structurally similar and the well-accepted constant curvature bending assumption [2, 5] was used in the kinematics modeling. The nomenclature and coordinates are defined in Section III.A, while the forward kinematics of a single continuum segment and the 6-DoF manipulator (excluding the DoF of the gripper) are derived in the Section III.B and Section III.C, respectively.

A. Nomenclature and Coordinates

Without loss of generality, the proposed dimension reduced method is applied to a 2-segment continuum manipulator from a previous study [8], as shown in Fig. 4(b). The base stem has two DoFs: feeding along and around its axis. Each continuum segment possesses two DoFs.

The coordinate attachments for the t^{th} segment and the entire manipulator are shown in Fig. 4(a) and Fig. 4(b), respectively. The corresponding definitions are as follows, while the nomenclature is listed in Table I, referring to [8, 9].

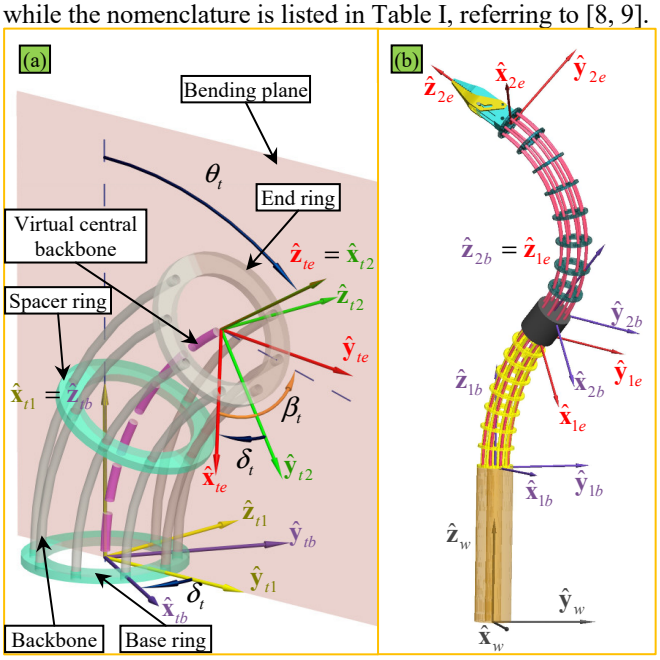

Fig. 4 Nomenclature and coordinates of: (a) the t^{th} continuum segment, and (b) the 6-DoF 2-continuum-segment manipulator [8].

TABLE I
NOMENCLATURE USED IN THE KINEMATICS MODELING

Symbol	*Definition*
t	Index of the segments, t = 1, 2, …, n.
L_t	Length of the virtual central backbone of the t^{th} segment.
θ_t	Bending angle of the t^{th} segment in the bending plane.
δ_t	For continuum segment, the right-handed rotation angle from bending plane to $\hat{\mathbf{x}}_{tb}$ about $\hat{\mathbf{z}}_{tb}$.
φ	Right-handed rotation angle of the base stem.
L_0, L_r, L_g	Length of the base stem, length of the rigid stem between the two continuum segments, and length of the gripper.
$\boldsymbol{\psi}_t$	$\boldsymbol{\psi}_t = [\theta_t\ \delta_t]^T$ is the configuration vector for t^{th} segment.
$\boldsymbol{\psi}_0$	$\boldsymbol{\psi}_0 = [L_0\ \varphi]^T$ is the configuration vector for the base stem.
$\boldsymbol{\psi}$	$\boldsymbol{\psi} = [\boldsymbol{\psi}_0^T\ \boldsymbol{\psi}_1^T\ \boldsymbol{\psi}_2^T]^T$ is the configuration vector for the entire 6-DoF manipulator.
${}^a\mathbf{R}_b$	The rotation matrix of frame $\{b\}$ with respect to $\{a\}$.
${}^a\mathbf{p}_b$	Position of the origin of coordinate $\{b\}$ or point b, with respect to the origin of coordinate $\{a\}$, with respect to coordinate $\{a\}$.
$\mathbf{J}_t$	Jacobian matrix mapping from configuration space to task space for segment t. $\mathbf{J}_t = [\mathbf{J}_{tv}^T\ \mathbf{J}_{t\omega}^T]^T$, where $\mathbf{J}_{tv}$ and $\mathbf{J}_{t\omega}$ are the linear and angular velocity items, respectively.

- *Base Coordinate* $\{tb\} \equiv \{\hat{\mathbf{x}}_{tb}, \hat{\mathbf{y}}_{tb}, \hat{\mathbf{z}}_{tb}\}$ locates its origin at the center of the base ring. $\hat{\mathbf{z}}_{tb}$ is perpendicular to the base ring and $\hat{\mathbf{x}}_{tb}$ points to the first backbone.
- *Bending Plane Coordinate 1* $\{t1\} \equiv \{\hat{\mathbf{x}}_{t1}, \hat{\mathbf{y}}_{t1}, \hat{\mathbf{z}}_{t1}\}$ is defined such that its *XY* plane is aligned with the bending plane of the *t*-th continuum segment with its origin coinciding with $\{tb\}$, and $\hat{\mathbf{x}}_{t1}$ aligned with $\hat{\mathbf{z}}_{tb}$.
- *Bending Plane Coordinate 2* $\{t2\} \equiv \{\hat{\mathbf{x}}_{t2}, \hat{\mathbf{y}}_{t2}, \hat{\mathbf{z}}_{t2}\}$ is obtained from $\{t1\}$ by a rotation about $\hat{\mathbf{z}}_{t1}$ with an angle θ_t. And the origin of $\{t2\}$ is attached at the center of the end disk and $\hat{\mathbf{x}}_{t2}$ is perpendicular to the end ring.
- *End Coordinate* $\{te\} \equiv \{\hat{\mathbf{x}}_{te}, \hat{\mathbf{y}}_{te}, \hat{\mathbf{z}}_{te}\}$ attaches its origin at the center of the end ring. $\hat{\mathbf{z}}_{te}$ aligns with $\hat{\mathbf{x}}_{t2}$. And $\hat{\mathbf{x}}_{te}$ is oriented to the first backbone.
- *World Coordinate* $\{w\} \equiv \{\hat{\mathbf{x}}_w, \hat{\mathbf{y}}_w, \hat{\mathbf{z}}_w\}$, is defined with $\hat{\mathbf{z}}_w$ aligned with the base stem. Furthermore, $\{1b\}$ is translated and rotated from $\{w\}$ along and around the $\hat{\mathbf{z}}_w$ with a length L_0 and an angle φ, consequently.

B. Forward Kinematics of the t^{th} Segment

The position vector from $\{tb\}$ to $\{te\}$ is as follows.

$$ {}^{tb}\mathbf{p}_{te} = \frac{L_t}{\theta_t}\begin{bmatrix}\cos\delta_t(1-\cos\theta_t) & \sin\delta_t(\cos\theta_t - 1) & \sin\theta_t\end{bmatrix}^T \quad (14) $$

When θ_t approaches 0, Eq. (14) approaches ${}^{tb}\mathbf{p}_{te} = [0\ 0\ L_t]^T$.

The orientation mapping from $\{tb\}$ to $\{te\}$ is as follows.

$$ {}^{tb}\mathbf{R}_{te} = {}^{tb}\mathbf{R}_{t1}\,{}^{t1}\mathbf{R}_{t2}\,{}^{t2}\mathbf{R}_{te} \quad (15) $$

Where ${}^{tb}\mathbf{R}_{t1} = \mathbf{R}_{\hat{\mathbf{z}}}(-\delta)\mathbf{R}_{\hat{\mathbf{x}}}(-\pi/2)\mathbf{R}_{\hat{\mathbf{z}}}(-\pi/2)$; $\mathbf{R}_{\hat{\mathbf{z}}}(-\delta)$ is a simple rotation about $\hat{\mathbf{z}}$ by an angle $-\delta$. Furthermore, ${}^{t1}\mathbf{R}_{t2} = \mathbf{R}_{\hat{\mathbf{z}}}(\theta)$, ${}^{t2}\mathbf{R}_{te} = {}^{tb}\mathbf{R}_{t1}^T$.

Jacobian matrix is derived as follows.

$$ \mathbf{J}_{tv} = L_t\begin{bmatrix} \cos\delta_t\left(\frac{\cos\theta_t - 1}{\theta_t^2} + \frac{\sin\theta_t}{\theta_t}\right) & \frac{\sin\delta_t}{\theta_t}(\cos\theta_t - 1) \\ \sin\delta_t\left(\frac{1-\cos\theta_t}{\theta_t^2} - \frac{\sin\theta_t}{\theta_t}\right) & \frac{\cos\delta_t}{\theta_t}(\cos\theta_t - 1) \\ -\frac{\sin\theta_t}{\theta_t^2} + \frac{\cos\theta_t}{\theta_t} & 0 \end{bmatrix} \quad (16) $$

$$ \mathbf{J}_{t\omega} = \begin{bmatrix} \sin\delta_t & \cos\delta_t & 0 \\ \cos\delta_t\sin\theta_t & -\sin\delta_t\sin\theta_t & \cos\theta_t - 1 \end{bmatrix}^T \quad (17) $$

When θ_t approaches 0, $\mathbf{J}_{tv}$ and $\mathbf{J}_{t\omega}$ can be derived according to L'Hôpital's rule.

Moreover, for the rigid stem $\mathbf{J}_{0v} = [\hat{\mathbf{z}}\ \mathbf{0}]$, $\mathbf{J}_{0\omega} = [\mathbf{0}\ \hat{\mathbf{z}}]$.

C. Kinematics of the 6-DoF Continuum Manipulator

The homogenous transformation from the World Coordinate to the tip of the gripper is expressed as follows.

$$ {}^w\mathbf{T}_g = {}^w\mathbf{T}_{1b}\,{}^{1b}\mathbf{T}_{1e}\,{}^{1e}\mathbf{T}_{2b}\,{}^{2b}\mathbf{T}_{2e}\,{}^{2e}\mathbf{T}_g \quad (18) $$

Where ${}^w\mathbf{T}_g := \begin{bmatrix} {}^w\mathbf{R}_g & {}^w\mathbf{p}_g \\ \mathbf{0} & 1 \end{bmatrix}$.

Besides the derivations in Section III.B, the rest orientation relationship between adjacent coordinates (or the tip of the gripper) can be expressed as ${}^w\mathbf{R}_{1b} = \mathbf{R}_{\hat{\mathbf{z}}}(\varphi)$, ${}^{1e}\mathbf{R}_{2b} = {}^{2e}\mathbf{R}_g = \mathbf{I}$. The position relationship can be simply formulated as ${}^w\mathbf{p}_{1b} = [0\ 0\ L_0]$, ${}^{1e}\mathbf{p}_{2b} = [0\ 0\ L_r]$, and ${}^{2e}\mathbf{p}_g = [0\ 0\ L_g]$.

The Jacobian of the 6-DoF manipulator with respect to the tip of the gripper can be derived as follows, in the World Coordinate.

$$ \mathbf{J}_m = \begin{bmatrix} \mathbf{T}_0 & {}^w\mathbf{R}_{1b}\mathbf{T}_1 & {}^w\mathbf{R}_{1b}\,{}^{1b}\mathbf{R}_{1e}\,{}^{1e}\mathbf{R}_{2b}\mathbf{T}_2 \\ \mathbf{J}_{0\omega} & {}^w\mathbf{R}_{1b}\mathbf{J}_{1\omega} & {}^w\mathbf{R}_{1b}\,{}^{1b}\mathbf{R}_{1e}\,{}^{1e}\mathbf{R}_{2b}\mathbf{J}_{2\omega} \end{bmatrix} \quad (19) $$

Where $\mathbf{T}_0 = \mathbf{J}_{0v} - ({}^w\mathbf{R}_{1b}\,{}^{1b}\mathbf{p}_g)^{\wedge}\mathbf{J}_{0\omega}$, $\mathbf{T}_1 = \mathbf{J}_{1v} - ({}^{1b}\mathbf{R}_{1e}\,{}^{1e}\mathbf{p}_g)^{\wedge}\mathbf{J}_{1\omega}$, and $\mathbf{T}_2 = \mathbf{J}_{2v} - ({}^{2b}\mathbf{R}_{2e}\,{}^{2e}\mathbf{p}_g)^{\wedge}\mathbf{J}_{2\omega}$. The operator $(\mathbf{p})^{\wedge}$ gives the skew-symmetric matrix of the vector $\mathbf{p}$.

The structural parameters and variable ranges are listed in Table II, which are kept consistent with the one in [8].

TABLE II
STRUCTURAL PARAMETERS AND VARIABLE RANGES

L_1 (mm)	L_r (mm)	L_2 (mm)	L_g (mm)	L_0 (mm)	θ_1 (rad)	θ_2 (rad)
40	20	60	20	[0,150]	[0,π/2]	[0,2π/3]

IV. NUMERICAL EXPERIMENTATIONS

Two representative case studies are reported in this section, comparing the conventional resolved motion rate control method and the proposed dimension-reduced method.

In both simulation case studies, both the initial and the target poses are within in the workspace of the 6-DoF continuum manipulator. The same pairs of the initial and the target configuration variables are used for both the conventional resolved motion rate control method and the dimension-reduced method to compare the different performances.

All the simulations were carried out in MATLAB 2016a on Windows 10 platform. In the task space, $v_{\mathbf{x}\text{lim}}$ is set at 100 mm/s, and $\omega_{\mathbf{x}\text{lim}}$ is set at $\pi/2$ rad/s. In the configuration space, the upper velocity limits for the prismatic and revolute configuration variables are set at 100 mm/s and $\pi/2$ rad/s, respectively. The time interval Δt is set at 1 ms. The error thresholds of position and orientation are 0.01 mm and 0.01 rad, respectively.

A. *Case Study One*

The initial and target poses are represented in the form of configuration variables, listed as #1 in Table III. The poses can be seen in Fig. 5(c).

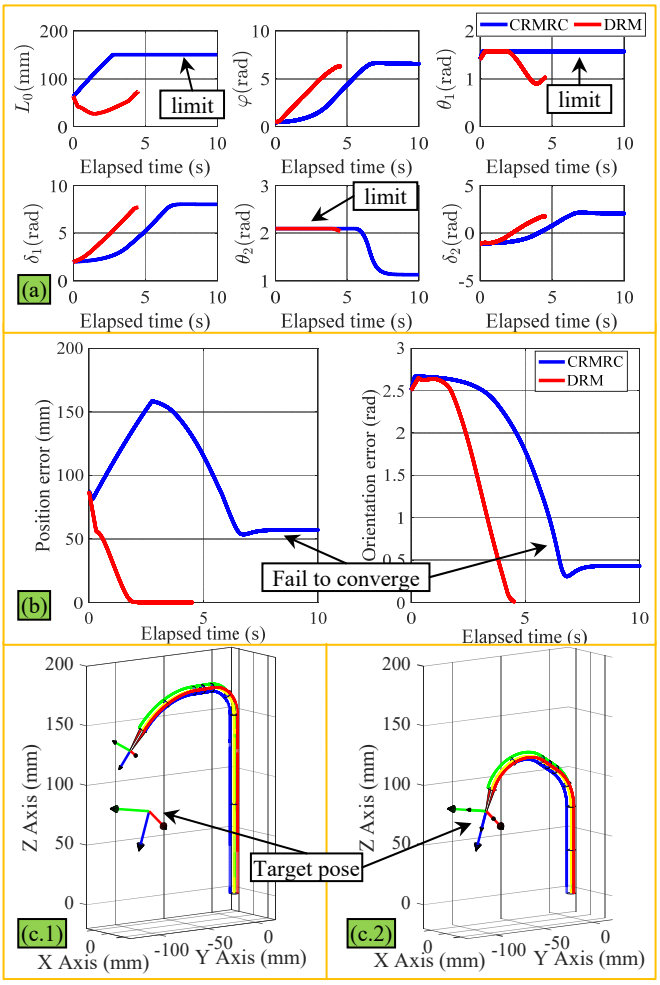

Fig. 5 The convergence comparison of the two methods: (a) trajectories of each configuration variable; (b) trajectories of the position and orientation errors; (c.1) the pose achieved by the CRMRC (conventional resolved motion rate control) after 10 s; and (c.2) the converged pose by DRM (dimension reduced method).

During the convergence of the conventional resolved motion rate control method, a large divergence occurs and the method fails to converge due to the fact that the configuration variable limits were encountered. However, properly using the movable DoFs that were not at their limits, the convergence continued in a proper way: the dimension reduced inverse kinematics method can quickly converge within the position and orientation error thresholds, with no deviation on the position errors throughout the entire process. Figure 5(a and b) shows the trajectories of each configuration variable and the position and orientation errors during the iterations, respectively. Figure 5(c.1) and Figure 5(c.2) illustrate the different poses obtained by the two methods.

B. *Case Study Two*

In the second case study, even though the initial pose is quite close to the target pose, the conventional resolved motion rate control method still fails to converge due to the configuration variable limits. The initial and the target configuration variables are listed as #2 in Table III, and the inverse kinematics process and the corresponding poses are shown in Fig. 6.

TABLE III
INITIAL AND TARGET CONFIGURATION VARIABLES

	L_0 (mm)	φ (rad)	θ_1 (rad)	δ_1 (rad)	θ_2 (rad)	δ_2 (rad)
Initial value #1	62.7827	0.4484	1.4036	1.9846	2.0943	-1.0885
Target value #1	74.0130	0.0147	1.0412	1.4377	2.0389	1.7679
Initial value #2	29.0030	-1.0068	1.3054	-1.3332	2.0943	-1.5215
Target value #2	41.8520	-1.0461	1.5276	-1.3863	2.0940	-1.5534

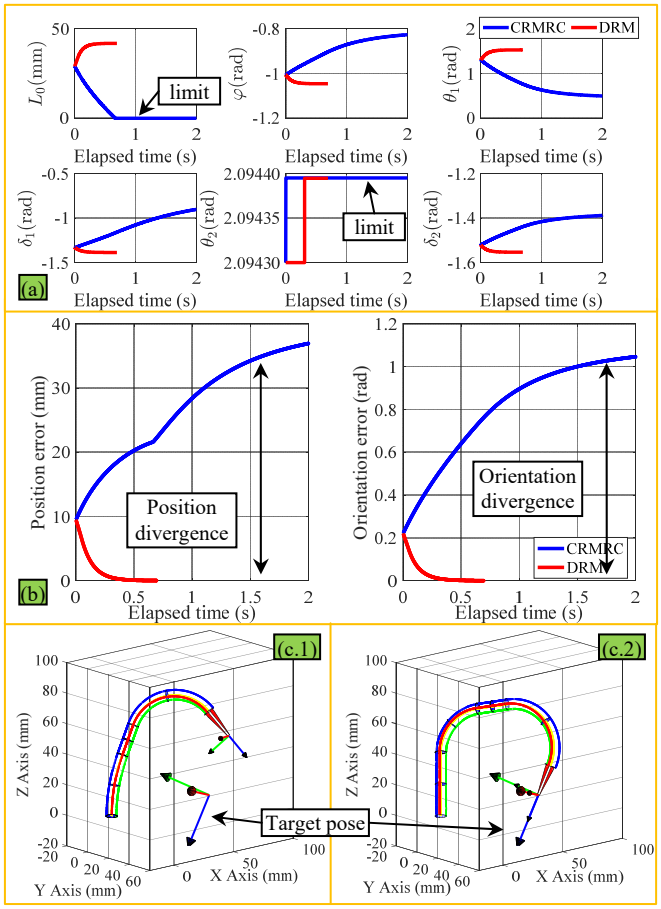

Fig. 6 The convergence comparison of the two methods: (a) trajectories of each configuration variable; (b) trajectories of the position and orientation errors; and (c) final poses obtained by CRMRC and DRM, respectively.

This simulation experiment further verifies the effectiveness of the proposed dimension reduced method in significantly avoiding positional divergence compared with the conventional method. It brings better performance around the configuration variable limits.

V. Conclusion and Future Work

Addressing the deficiency when the conventional resolved motion rate control method handles the configuration variable limits, this paper introduces a dimension-reduced method to provide numerical stability. The proposed method essentially uses the non-saturated configuration variables to provide a least-square motion solution for a desired motion twist. Since it is highly possible that the desired task twist cannot be satisfied completely, a prioritized formulation is adopted to set the desired linear velocity at a higher priority with respect to the angular velocity. To avoid excessive configuration velocities, a scaling-down modification is also introduced.

The proposed method can help maintain numerical stability for the Jacobian-based instantaneous inverse kinematics around configuration variable limits. Even around the configuration variable limits, the iterative process can still continue without bringing a divergence.

Numerical experiments were conducted to demonstrate that the proposed dimension-reduced inverse kinematics method appears to have significant strengths compared to the conventional Jacobian-based method.

Extensive experiments on these advantages shall be verified in the near future, in order to fully evaluate the effectiveness of the proposed method.

References

[1] G. Robinson and J. B. Davies, "Continuum Robots - A State of the Art," in *IEEE International Conference on Robotics and Automation (ICRA)*, Detroit, Michigan, 1999, pp. 2849-2853.

[2] R. J. Webster and B. A. Jones, "Design and Kinematic Modeling of Constant Curvature Continuum Robots: A Review " *International Journal of Robotics Research,* vol. 29, No.13, pp. 1661-1683, Nov 2010.

[3] J. Burgner-Kahrs, D. C. Rucker, and H. Choset, "Continuum Robots for Medical Applications: A Survey," *IEEE Transactions on Robotics,* vol. 31, No.6, pp. 1261-1280, Dec 2015.

[4] J. Zhao, B. Feng, M.-H. Zheng, and K. Xu, "Surgical Robots for SPL and NOTES: a Review," *Minimally Invasive Therapy and Allied Technologies,* vol. 24, No.1, pp. 8-17, Jan 2015.

[5] K. Xu and N. Simaan, "Analytic Formulation for the Kinematics, Statics and Shape Restoration of Multibackbone Continuum Robots via Elliptic Integrals," *Journal of Mechanisms and Robotics,* vol. 2, No.011006, pp. 1-13, Feb 2010.

[6] W. Zhang, Z. Yang, T. Dong, and K. Xu, "FABRIKc: An Efficient Iterative Inverse Kinematics Solver for Continuum Robots," in *IEEE/ASME International Conference on Advanced Intelligent Mechatronics (AIM)*, Auckland, New Zealand, 2018, pp. 346-352.

[7] D. E. Whitney, "Resolved Motion Rate Control of Manipulators and Human Prostheses," *IEEE Transactions on Man-Machine Systems,* vol. 10, No.2, pp. 47-53, June 1969.

[8] S. a. Zhang, Y. Chen, Q. Li, B. Zhao, and K. Xu, "Kinematic Optimization of a Continuum Surgical Manipulator," in *IEEE International Conference on Robotics and Biomimetics (ROBIO)*, Kuala Lumpur, Malaysia, 2018, pp. 2069-2074.

[9] K. Xu, J. Zhao, and M. Fu, "Development of the SJTU Unfoldable Robotic System (SURS) for Single Port Laparoscopy," *IEEE/ASME Transactions on Mechatronics,* vol. 20, No.5, pp. 2133-2145, Oct 2015.

[10] S. Liu, Z. Yang, Z. Zhu, L. Han, X. Zhu, and K. Xu, "Development of a Dexterous Continuum Manipulator for Exploration and Inspection in Confined Spaces," *Industrial Robot: An International Journal,* vol. 43, No.3, pp. 284-295, 2016.

[11] K. Xu, B. Liang, Z. Dai, J. Zhao, B. Zhao, H. Liu, L. Xiao, and Y. Sun, "Preliminary Development of a Continuum Dual-Arm Surgical Robotic System for Transurethral Procedures," in *International Conference on Intelligent Robotics and Applications (ICIRA)*, Wuhan, China, 2017, pp. 311-322.

[12] T. F. Chan and R. V. Dubey, "A Weighted Least-Norm Solution Based Scheme for Avoiding Joint Limits for Redundant Joint Manipulators," *IEEE Transactions on Robotics and Automation,* vol. 11, No.2, pp. 286-292, April 1995.

[13] L. Sciavicco and B. Siciliano, "A Solution Algorithm to the Inverse Kinematic Problem for Redundant Manipulators," *IEEE Journal on Robotics and Automation,* vol. 4, No.4, pp. 403-410, Aug. 1988.

[14] F. Flacco, A. De Luca, and O. Khatib, "Control of Redundant Robots Under Hard Joint Constraints: Saturation in the Null Space," *IEEE Transactions on Robotics,* vol. 31, No.3, pp. 637-654, June 2015.

[15] A. Colomé and C. Torras, "Closed-Loop Inverse Kinematics for Redundant Robots: Comparative Assessment and Two Enhancements," *IEEE/ASME Transactions on Mechatronics,* vol. 20, No.2, pp. 944-955, June 2015.

[16] D. N. Nenchev, "Restricted Jacobian Matrices of Redundant Manipulators in Constrained Motion Tasks," *The International Journal of Robotics Research,* vol. 11, No.6, pp. 584-597, 1992.